THE JOURNAL OF PHYSICAL CHEMISTRY B
A JOURNAL OF THE AMERICAN CHEMICAL SOCIETY

pubs.acs.org/JPCB

Article

Mechanistic Picture for Monomeric Human Fibroblast Growth Factor 1 Stabilization by Heparin Binding

Vivek Govind Kumar, Shilpi Agrawal, Thallapuranam Krishnaswamy Suresh Kumar, and Mahmoud Moradi*

Cite This: *J. Phys. Chem. B* 2021, 125, 12690–12697

Read Online

ACCESS | Metrics & More | Article Recommendations | Supporting Information

ABSTRACT: Human fibroblast growth factor (FGF) 1 or hFGF1 is a member of the FGF family that is involved in various vital processes such as cell proliferation, cell differentiation, angiogenesis, and wound healing. hFGF1, which is associated with low stability *in vivo*, is known to be stabilized by binding heparin sulfate, a glycosaminoglycan that aids the protein in the activation of its cell surface receptor. The poor thermal and proteolytic stability of hFGF1 and the stabilizing role of heparin have long been observed experimentally; however, the mechanistic details of these phenomena are not well understood. Here, we have used microsecond-level equilibrium molecular dynamics (MD) simulations to quantitatively characterize the structural dynamics of monomeric hFGF1 in the presence and absence of heparin hexasaccharide. We have observed a conformational change in the heparin-binding pocket of hFGF1 that occurs only in the absence of heparin. Several intramolecular interactions were also identified within the heparin-binding pocket that form only when hFGF1 interacts with heparin. The loss of both intermolecular and intramolecular interactions in the absence of heparin plausibly leads to the observed conformational change. This conformational transition results in increased flexibility of the heparin-binding pocket and provides an explanation for the susceptibility of *apo* hFGF1 to proteolytic degradation and thermal instability. This study provides a glimpse into mechanistic details of the heparin-mediated stabilization of hFGF1 and encourages the use of microsecond-level MD in studying the effect of binding on protein structure and dynamics. In addition, the observed differential behavior of hFGF1 in the absence and presence of heparin provides an example, where microsecond-level all-atom MD simulations are necessary to see functionally relevant biomolecular phenomena that otherwise will not be observed on sub-microsecond time scales.

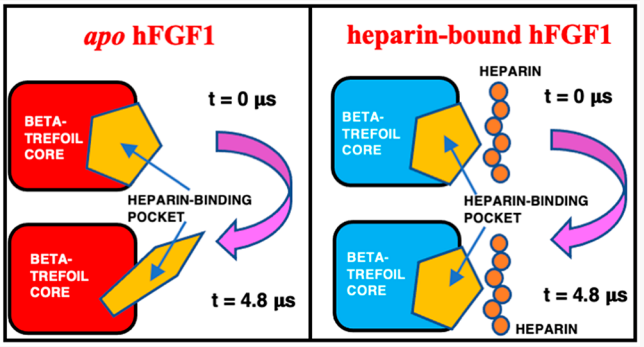

INTRODUCTION

Thanks to the ever-increasing power of computers, improved force fields, and high-throughput modeling, all-atom molecular dynamics (MD) is now routinely used to simulate proteins in simplified but explicit aqueous/membrane environments. MD simulations combine the high spatial resolution of experimental methods such as X-ray crystallography with the high temporal resolution of experimental methods such as single-molecule FRET spectroscopy.[1,2] However, many MD studies implicitly assume that local conformational transitions observed in short, nanosecond-level simulations can be used to describe global protein conformational transitions that typically occur on microsecond or millisecond time scales.[3,4] We have recently demonstrated that longer microsecond-level simulations are essential for a more precise statistical characterization of both local and global conformational transitions.[5] Here, we use microsecond-level unbiased MD simulations to investigate the conformational and structural dynamics of monomeric hFGF1[6] and the chemo-mechanical coupling between hFGF1 and heparin, its glycosaminoglycan (GAG) binding partner.

Fibroblast growth factors (FGFs) are signaling proteins that are involved in an extensive variety of physiological processes.[7−9] The biological activity of FGFs is regulated through interactions with linear anionic polysaccharides called glycosaminoglycans (GAGs), which facilitate binding to specific receptors on the cell surface (FGFRs).[10−17] Human acidic fibroblast growth factor (hFGF1) is an important signaling molecule expressed in embryonic and adult tissues for angiogenesis, cell proliferation and differentiation, tumor growth, neurogenesis and wound healing.[10,18] Glycosaminoglycans (GAGs) consist of a class of negatively charged and

Received: September 2, 2021
Revised: October 20, 2021
Published: November 11, 2021

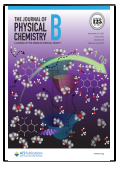

https://doi.org/10.1021/acs.jpcb.1c07772
J. Phys. Chem. B 2021, 125, 12690–12697

large linear polysaccharides formed of repeating disaccharide units in which a uronic acid (either glucuronic acid or iduronic acid) moiety is combined with an amino sugar (either *N-acetyl*-D-glucosamine or *N-acetyl*-D-galactosamine).[19,20] Heparin is a GAG made up of 2-*O*-sulfated iduronic acid and 6-*O*-sulfated, N-sulfated glucosamine (IdoA(2S)-GlcNS(6S)), connected by α-(1→4) glycosidic linkages.[21] The anionic nature of GAGs leads to electrostatic interactions with positively charged (lysine-/arginine-rich) regions of their target proteins.[19,20] The hFGF1−heparin complex is the most broadly studied protein-GAG complex.[22,23]

The interaction of hFGF1 with specific heparin sulfate proteoglycans may be influenced by the flexibility of the heparin-binding pocket.[24] In addition to the structural features of hFGF1, GAG sulfation patterns also determine the functionality and specificity of protein−GAG interactions.[25,26] hFGF1 is known to selectively recognize the GlcNS-IdoA2S-GlcNS sulfation motif.[27] DiGabriele et al.[28] crystallized a dimeric hFGF1−heparin sandwich complex (Protein Data Bank (PDB) entry: 2AXM) and showed that heparin binding does not result in any global conformational changes within hFGF1.[28,29] Solution nuclear magnetic resonance (NMR) and experimental binding studies suggest that a monomeric hFGF1−heparin complex is also fully functional.[23,30] *apo* hFGF1 shows relatively low thermal stability and is known to be susceptible to thermal degradation.[31,32] Binding to heparin sulfate proteoglycans is thought to protect hFGF1 against proteolytic degradation.[33,34]

Our microsecond-level all-atom equilibrium MD simulations reveal that a conformational change occurs in the heparin-binding pocket of hFGF1 in the absence of heparin. We postulate that this conformational change is responsible for the susceptibility of unbound hFGF1 to thermal instability, as seen in equilibrium unfolding experiments. We have also studied the intermolecular interactions of the hFGF1−heparin complex and the intramolecular interactions that are unique to heparin-bound hFGF1 in order to obtain a clearer picture of the heparin-mediated stabilization.

METHODS

Equilibrium Unfolding of hFGF1 with Heparin Hexasaccharide. The temperature-based denaturation experiment was conducted using the JASCO-1500 circular dichroism spectrophotometer connected with a fluorescence detector. hFGF1 was diluted with 10 mM phosphate buffer containing 100 mM NaCl at pH 7.2 to get a concentration of 33 μM. The experiment was conducted with and without heparin. For the measurements with heparin, protein to heparin ratio of 1:10 was used. The fluorescence spectra were collected in 5 °C intervals from 25 to 90 °C. The fraction of denatured protein (F_d) at each temperature was determined as $F_d = (Y - Y_N)/(Y_D - Y_N)$, where Y, Y_N, and Y_D are the fluorescence signals of the 305/350 nm fluorescence ratio at the native state (25 °C), each consecutive temperature, and the denatured state (90 °C) respectively. The data set was fit using MS Excel. T_m, the temperature at which 50% of the protein molecules exist in the denatured state(s), was calculated from the fraction denatured protein population versus temperature graph.

All-Atom Equilibrium MD Simulations. We have used all-atom equilibrium MD simulations to characterize the conformational dynamics of hFGF1 with and without heparin hexasaccharide. Our simulations were based on the X-ray crystal structures of the unbound hFGF1 monomer (PDB: 1RG8, resolution: 1.1 Å)[6] and the dimeric complex with a heparin hexasaccharide (PDB: 2AXM, resolution: 3.0 Å).[28] We built three different models: monomeric *apo* hFGF1 from 1RG8; monomeric heparin-bound hFGF1 (1RG8) using the heparin hexasaccharide from the dimeric complex (2AXM) (Model 1), and monomeric heparin-bound hFGF1 from the dimeric complex (2AXM) (Model 2). Residues 12−137 in the PDB files correspond to residues 26−151 in the experimental sequence. The experiments were conducted using a truncated version of hFGF1 (residues 13−154) which did not contain the unstructured 12 amino acid N-terminal segment. The unstructured N-terminal segment is not known to be involved in receptor activation or heparin binding. The heparin hexasaccharide consists of *N*,*O*6-disulfo-glucosamine and 2-*O*-sulfo-alpha-L-idopyranuronic acid repeats.[28]

MD simulations were conducted using the NAMD 2.13[35] simulation package with the CHARMM36 all-atom additive force field.[36] The input files for energy minimization and production were generated using CHARMM-GUI.[37,38] For heparin-bound Model 1, the heparin hexasaccharide segment from 2AXM was added to the 1RG8 structure using psfgen. The models were then solvated in a box of TIP3P waters and 0.15 M NaCl. The heparin-bound systems had approximately 23 000 atoms, while the *apo* system had 27 000 atoms.

Initially, we energy-minimized each system for 10 000 steps using the conjugate gradient algorithm.[39] Subsequently, we relaxed the systems using restrained MD simulations in a stepwise manner (for a total of ∼1 ns) using the standard CHARMM-GUI protocol.[37] The initial relaxation was conducted in an *NVT* ensemble, while all production runs were conducted in an *NPT* ensemble. Simulations were carried out using a 2 fs time step at 300 K using a Langevin integrator with a damping coefficient of γ = 0.5 ps^{-1}. The pressure was maintained at 1 atm using the Nosé−Hoover Langevin piston method.[39,40] The smoothed cutoff distance for nonbonded interactions was set to 10−12 Å, and long-range electrostatic interactions were computed with the particle mesh Ewald (PME) method.[41] The initial production run for each model lasted 15 ns, in which the conformations were collected every 2 ps. After each model was equilibrated for 15 ns, the production runs were extended on the supercomputer Anton 2 (Pittsburgh Supercomputing Center) for 4.8 μs each, with a time step of 2.5 fs. Conformations were collected every 240 ps.

VMD[42] was used to analyze the simulation trajectories. The root-mean-square deviation (RMSD) Trajectory tool[42] was used to calculate the RMSD and C_α atoms were considered for these calculations. For internal RMSD, the region of interest was aligned against its own initial configuration and RMSD was calculated with respect to this configuration. The root-mean-square fluctuation (RMSF) values of individual residues were calculated using the C_α atoms by aligning the trajectory against the crystal structure. The HBond[42] and Salt Bridge[42] plugins were used to generate the data for hydrogen bonding and salt-bridge analysis, respectively. For all interactions of interest, the number of frames with 1 or more hydrogen bonds was counted to get the occupancy percentage. An occupancy cutoff of 50%, a donor−acceptor distance cutoff of 4 Å, and an angle cutoff of 35° were used to define hydrogen bond/salt bridge interactions. The salt-bridge plugin[42] was used to calculate the distance between the two salt-bridge residues over the course of the simulation, which is the distance between the oxygen atom of the participating acidic residue and the

https://doi.org/10.1021/acs.jpcb.1c07772
J. Phys. Chem. B 2021, 125, 12690−12697

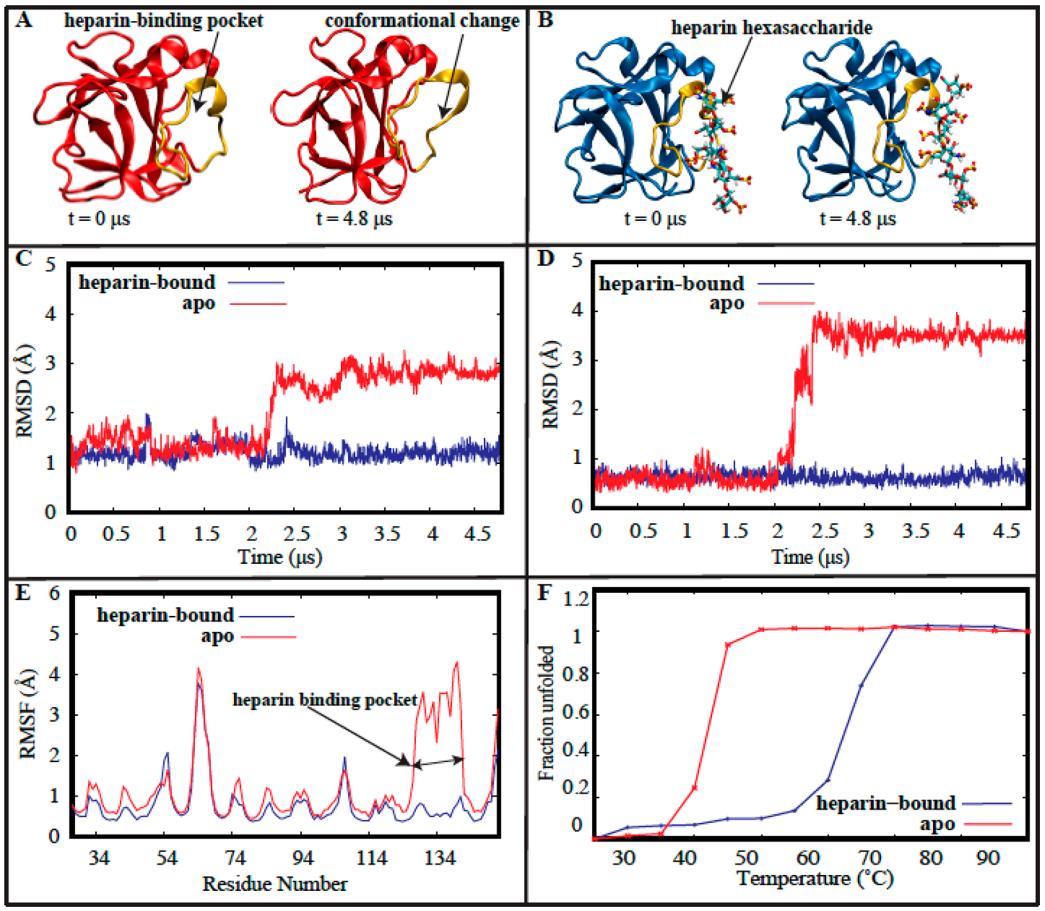

Figure 1. Conformational change in the heparin-binding pocket of*apo*hFGF1. (A, B) Cartoon representation of *apo* (red) and heparin-bound (blue) hFGF1 at the beginning and end of the 4.8-μs simulations. The heparin-binding pocket (gold) moves away from the beta-trefoil core of the *apo* protein. (C, D) RMSD time series for the *apo* (red) and heparin-bound (blue) models of hFGF1 protein (C) and its heparin binding pocket (D). (E) RMSF estimations for the *apo* (red) and heparin-bound (blue) models of hFGF1. (F) Thermal denaturation data for hFGF1 in the absence (red) and presence (blue) of heparin. The presence of heparin causes the T_m value to increase by around 20 °C, indicating that heparin stabilizes the protein.

nitrogen atom of the basic residue. The Timeline plugin[42] was used to analyze protein secondary structure. An internal measurement method in VMD was used to count the number of water molecules within 3 Å of the heparin-binding pocket.[42]

RESULTS AND DISCUSSION

The putative role of heparin is to prevent the degradation of hFGF1. However, the specifics of this heparin-mediated stabilization are still unclear. To address this issue, we have used microsecond-level all-atom MD to compare and characterize the *apo* and heparin-bound forms of hFGF1.

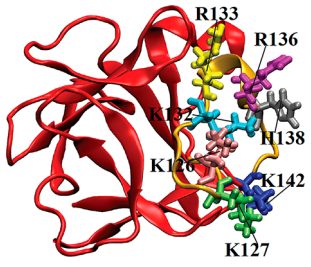

Figure 2. Cartoon representation of *apo*hFGF1. The positively charged residues of the heparin-binding pocket (gold) are shown using stick representation. These residues are involved in both intramolecular and intermolecular electrostatic interactions.

We have conducted three unbiased all-atom MD simulations of monomeric hFGF1, each for 4.8 μs. One *apo* and two heparin-bound models were simulated in the presence of explicit water. The *apo* model and one of the heparin-bound models (Model 1) are based on the crystal structure of monomeric *apo* hFGF1 (PDB entry: 1RG8).[6] In order to examine the reproducibility of our results, we have also made a second heparin-bound model of hFGF1. The second heparin-bound model is extracted as a monomeric model from the crystal structure of dimeric heparin-bound hFGF1 (PDB entry: 2AXM)[28] (Figure S1). Both heparin-bound models use a heparin hexasaccharide. The heparin-bound models are quite similar and involve an hFGF1 monomer bound to heparin hexasaccharide. As the only difference between the *apo* and heparin-bound models is the presence or absence of heparin, we can make meaningful comparisons between all three sets of simulations (i.e., two *holo* and one *apo* models).

Conformational Change Occurs in the Heparin-Binding Pocket of the *apo* Model. The most noticeable observation in our simulations is that the heparin-binding pocket (residues 126−142) of the *apo* model becomes elongated and extends further outward and away from the core beta-trefoil structure after approximately 2 μs (Figure

https://doi.org/10.1021/acs.jpcb.1c07772
J. Phys. Chem. B 2021, 125, 12690−12697

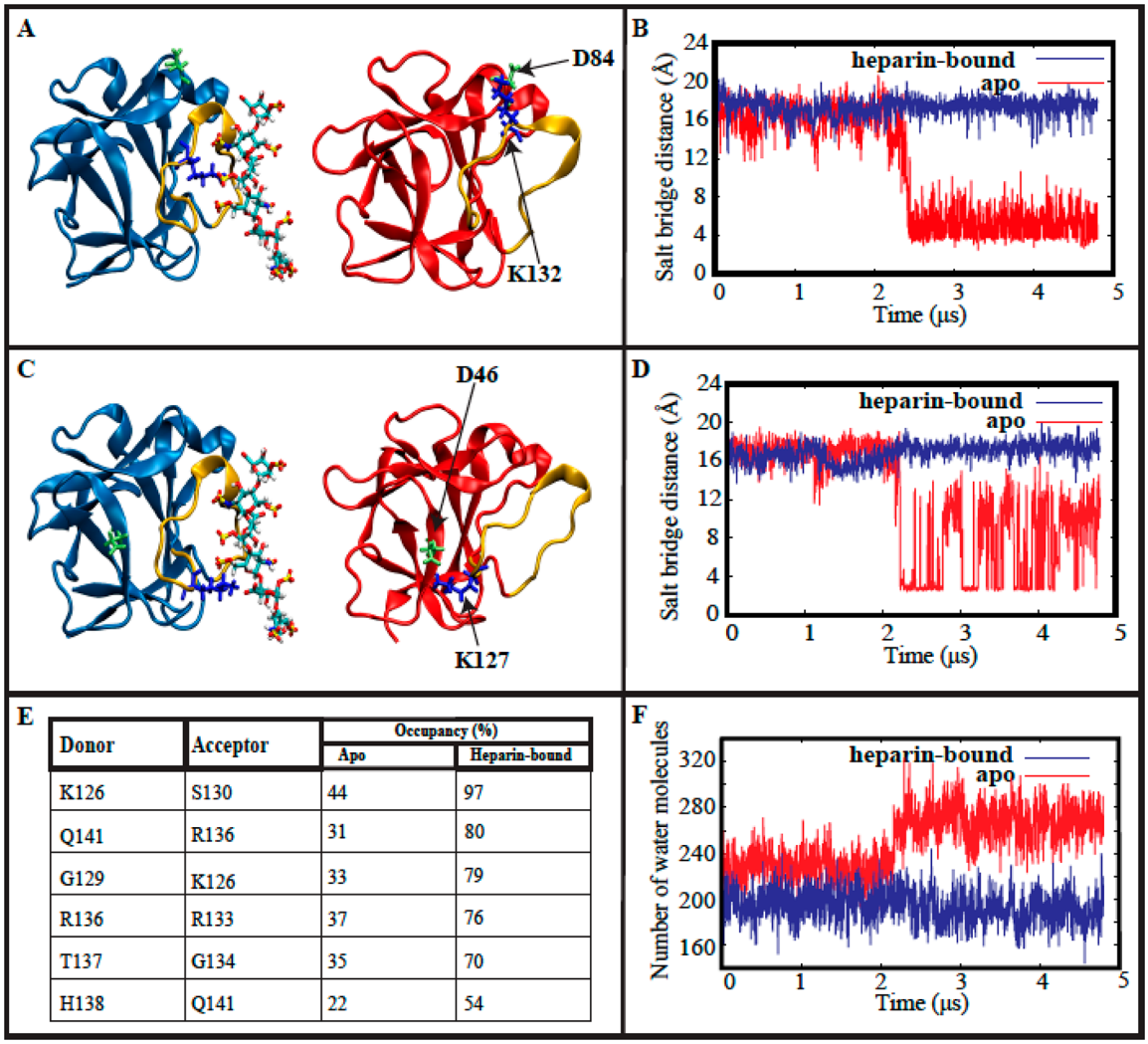

Donor	Acceptor	Occupancy (%)	
		Apo	Heparin-bound
K126	S130	44	97
Q141	R136	31	80
G129	K126	33	79
R136	R133	37	76
T137	G134	35	70
H138	Q141	22	54

Figure 3. Unique salt-bridge interactions facilitate the conformational change in the *apo* model. (A) K132 (blue) of the heparin-binding pocket (gold) forms a salt-bridge with D84 of the beta-trefoil core in the *apo* model (red). This interaction does not form in the heparin-bound protein (blue). (B) Time series of the D84-K132 donor−acceptor salt bridge distances in the presence (blue) and absence (red) of heparin. (C) K127 (blue) of the heparin-binding pocket (gold) forms a weak salt-bridge with D46 of the beta-trefoil core in the *apo* model (red). This interaction does not form in the heparin-bound Model 1 (blue). (D) Time series of the D46-K127 donor−acceptor salt bridge distances in the presence (blue) and absence (red) of heparin. (E) Table of intramolecular interactions unique to the heparin-binding pocket of heparin-bound hFGF1. (F) Time series of water molecule count within 3 Å of the heparin-binding pocket.

1A). This conformational change is not observed in either of the two heparin-bound models (Figures 1B and S2A). Comparing the internal RMSD of the hFGF1 monomer from each system reveals that the presence of heparin hexasaccharide stabilizes the protein and prevents this conformational change from occurring (Figures 1C and S2A,B). All 3 models initially have internal RMSD values of approximately 1 Å from their initial conformations, indicating little flexibility at least within the first 2 μs of simulations. Both heparin-bound models settle down into a stable conformation within 0.5 μs (RMSD = 1.5−2 Å approximately) (Figures 1C and S2A,B). However, the *apo* model clearly undergoes a conformational change after 2 μs (RMSD = 3 Å approx.) (Figure 1C,A). This new conformation then remains stable for the remainder of the simulation (around 2.8 μs) (Figure 1C,A).

A comparison of the internal RMSD of the heparin-binding pocket reveals that this region plays a key role in the differential behavior of the *apo* (RMSD ≈ 4 Å) and heparin-bound models (RMSD ≈ 0.5 Å) (Figures 1D and S2C,D). This indicates that the absence of interactions with heparin leads to the decreased stability of the *apo* model. These results are also supported by the RMSF data for each model, which was calculated for the C_α atoms of all protein residues (Figure 1E and S2E,F). All three models show similar trends in the fluctuations for different regions, with the exception of the heparin-binding pocket. As expected, the heparin-binding pocket is much more flexible in the *apo* model than in the heparin-bound models.

Thermal denaturation experiments were conducted on monomeric hFGF1, in the absence and presence of heparin hexasaccharide, to further validate our computational results. The T_m value for the *apo* experimental model was approximately 42 °C, while the T_m value for the heparin-bound experimental model was approximately 62.5 °C (Figure 1F). The presence of heparin thus increases the T_m value by around 20 °C, indicating that heparin stabilizes the protein.

https://doi.org/10.1021/acs.jpcb.1c07772
J. Phys. Chem. B 2021, 125, 12690−12697

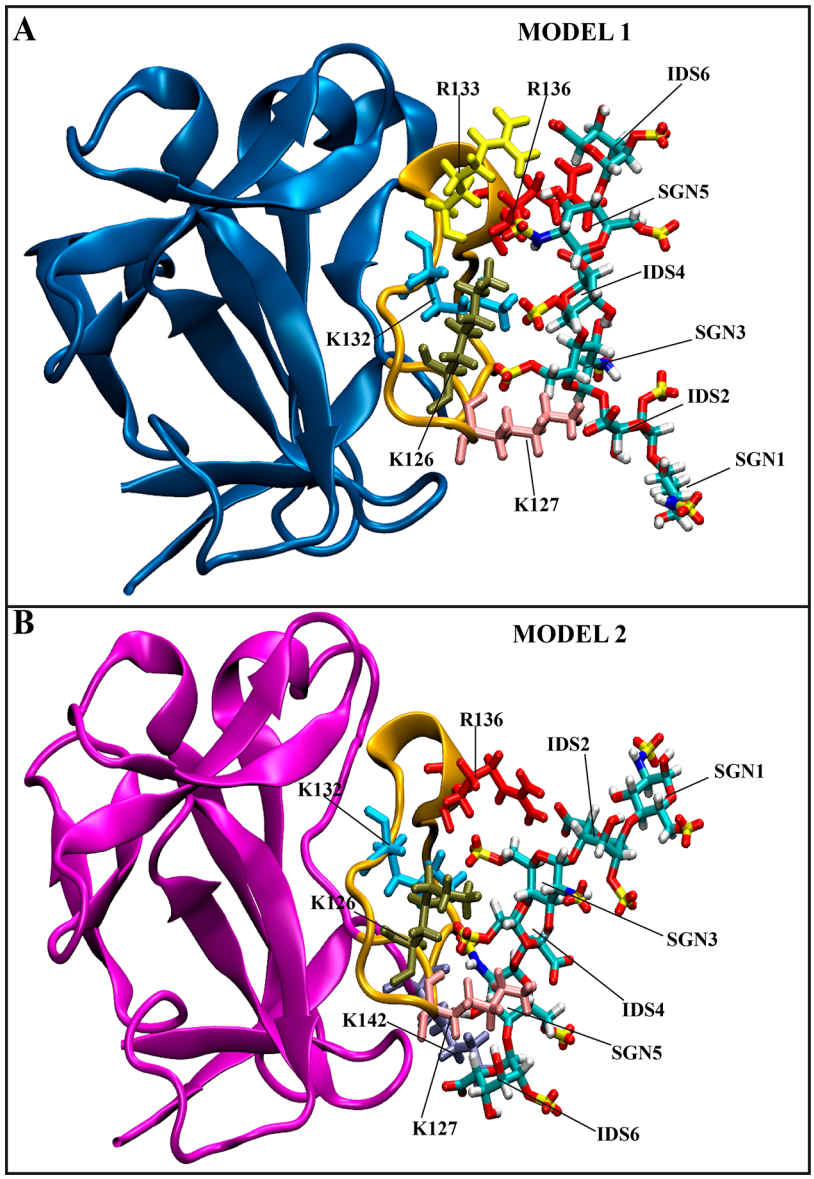

Figure 4. Cartoon representation of the final frames of the two heparin-bound trajectories. (A) Model 1 (blue): heparin hexasaccharide from PDB entry 2AXM with monomeric hFGF1 from PDB entry 1RG8. (B) Model 2 (magenta): one monomer and heparin hexasaccharide from 2AXM (dimeric). Six residues in the heparin-binding pocket (R136, K132, K126, K127, R133, and K142) were found to interact with heparin hexasaccharide.

These observations are in qualitative agreement with the computational RMSD/RMSF data.

Unique Salt-Bridge Interactions Facilitate the Conformational Change in the *apo* Model. The conformational change that occurs in the *apo* model is localized in the heparin-binding pocket. Electrostatic interactions between positively charged residues in the heparin-binding pocket (Figure 2) and negatively charged residues in the beta-trefoil core help stabilize the new conformation. We have identified two salt bridge interactions that are unique to the *apo* model. They do not form in the two heparin-bound models (Figure 3A−D and S3A−D). D84 of the beta-trefoil core interacts with K132 of the heparin-binding pocket (Figure 2 and 3A,B), while D46 of the beta-trefoil core interacts with K127 of the heparin-binding pocket (Figures 2 and 3C,D). The destabilization of the heparin-binding pocket is accompanied by the formation of a weak salt bridge between D46 and K127 (Figure 3C−D), followed by the formation of a stronger salt bridge between D84 and K132 when the heparin-binding pocket becomes elongated and is extended outward (Figure 3A,B) and away from the beta-trefoil core. Both K127 and K132 are known to interact with negatively charged heparin residues.[30] Interactions with negatively charged residues of the beta-trefoil core possibly compensate for the absence of interactions with heparin. Together, these salt bridges play a key role in stabilizing the new conformation of the heparin-binding pocket for almost 2.8 μs.

Hydration analysis of the heparin-binding pocket (quantified by the number of water molecules within 3 Å of this domain) provides additional evidence for a conformational change within the heparin-binding pocket. Around 200 water molecules are present throughout both heparin-bound trajectories (Figures 3F and S3E,F). During the *apo* simulation, however, the count of water molecules increases to 280 after 2

https://doi.org/10.1021/acs.jpcb.1c07772
J. Phys. Chem. B 2021, 125, 12690−12697

Table 1. Characterization of the hFGF1−Heparin Intermolecular Interactions in the Heparin Binding Pocket[a]

	Acceptor	
donor	Model 1	Model 2
R136	IDS4 (78%)	IDS2 (91%)
K126	SGN5 (68%) IDS4 (51%)	SGN3 (75%) IDS4 (72%)
K132	SGN3 (53%)	SGN3 (66%) IDS4 (52%)
K127	SGN3 (54%) IDS2 (61%)	IDS4 (75%)
R133	IDS6 (57%) SGN5 (64%)	none
K142	none	SGN5 (85%) IDS6 (57%)

[a]Intermolecular hydrogen-bonding interactions observed in the last microsecond of both heparin-bound trajectories. R133 interacts with heparin only in Model 1, while K142 interacts with heparin only in Model 2.

μs (Figure 3F), thus coinciding with the observed conformational change.

Intramolecular Interactions within the Heparin-Binding Pocket Help Stabilize Heparin-Bound hFGF1. Thus, far, we have shown that monomeric hFGF1 is destabilized in the absence of heparin and that a conformational change occurs within the heparin-binding pocket. This conformational change does not occur in the heparin-bound models, which are considerably more stable than the *apo* model. We have identified several unique intramolecular interactions within the heparin-binding pocket that contribute to the increased stability of the heparin-bound hFGF1 models (Figures 3E and S4). Hydrogen bond occupancies are quite similar in both Models 1 and 2 (Figure 3E and S4). While these interactions are also present briefly in the *apo* model, none of them meet the occupancy criteria that would allow them to be described as hydrogen bonds (Figure 3E). We propose that these intramolecular interactions within the protein may form as a consequence of intermolecular interactions between positively charged residues of the heparin-binding pocket (Figure 2) and negatively charged residues of heparin hexasaccharide. The strength of these intramolecular interactions (occupancies between 54 and 97% in Model 1 and 64−94% in Model 2) might thus be a factor that prevents the conformational change observed in the *apo* model from occurring in the heparin-bound models. Among intramolecular hydrogen bonds observed in the *apo* model, only one (L145−K142) involves the heparin-binding pocket (occupancy: 84%). All of the interactions observed in the *apo* model, including salt bridges D46-R38 (90%), D53-R38 (87%), and E67-K114 (60%), also occur in the heparin-bound models with similar occupancies.

Secondary structure analysis reveals that parts of the heparin-binding pocket of the *apo* model become unstructured and unravel into random coils when the conformational change occurs (Figure S5A,B). This change in the secondary structure is then maintained for the remaining 2.8 μs of the *apo* trajectory. This change in the secondary structure is not observed in the heparin-bound models (Figure S5C,D). The lack of strong intramolecular interactions in the heparin-binding pocket of the *apo* model (Figure 3E) could thus account for the observed changes in the secondary structure.

Our findings are further validated by internal RMSD analysis of the heparin-binding pocket of the *apo* (RMSD of ∼4 Å) and heparin-bound (RMSD of ∼0.5 Å) models (Figures 1D and S2C,D). This analysis demonstrates that the heparin-binding pockets of *apo* and heparin-bound hFGF1 have different internal conformations. Therefore, these observations confirm the role of heparin-derived intramolecular interactions in maintaining and promoting the structured nature of the heparin-binding pocket.

Characterization of Intermolecular Interactions That Contribute to the Stabilizing Effects of Heparin. The heparin hexasaccharide in Model 1 fluctuates considerably before it eventually undergoes a 180° rotation to settle down into a more stable conformation (Figure S6A). This transition occurs at the 1.25 μs mark and continues until the 2 μs mark (Figure S6A). In contrast, the heparin molecule in Model 2 does not undergo any major positional changes and attains a stable conformation very quickly (Figure S6B). As a result of the differences in behavior and position of the heparin hexasaccharide in each model, slightly different intermolecular bond interactions occur in each model in terms of both occupancy as well as the residues involved (Figure 4, Table 1). Six residues in the heparin-binding pocket (R136, K132, K126, K127, R133, and K142) were found to be involved in these interactions (Figure 4A,B). With the exception of R133, intermolecular hydrogen bonds involving these residues are present in the dimeric crystal structure (PDB entry: 2AXM).[28] R133 was found to interact with heparin only in Model 1 (Figure 4A), while K142 was found to interact with heparin only in Model 2 (Figure 4B). Intermolecular interactions involving N32, N128, and Q141 are also present in the dimeric crystal structure[28] but these residues only interact briefly (hydrogen bond occupancies <35%) with heparin in our simulation trajectories.

Occupancies are fairly similar for interactions involving R136 and K126 in both models, while they are somewhat different for interactions involving residues K132 and K127. R133 and K142 only interact with heparin hexasaccharide in Models 1 and 2, respectively. See Table 1 and Figure S7 for more details. As discussed previously, we have also identified six major intramolecular interactions within the heparin-binding pocket that are unique to heparin-bound hFGF1 (Figures 3E and S4). The presence of heparin ostensibly leads to the formation of these intramolecular hydrogen bonds, which consequently contribute to the stabilization of heparin-bound hFGF1. This is consistent with the thermal denaturation experiments described above, where the T_m value increases by around 20 °C upon heparin binding (Figure 1F), indicating an increase in the strength of protein intramolecular interactions upon heparin binding.

CONCLUSIONS

In this study, we used microsecond-level MD simulations to compare the behavior of hFGF1 in the absence and presence of heparin hexasaccharide at the molecular level. These simulations reveal a significant conformational difference within the heparin-binding pocket in the absence and presence of the ligand. We conclude that the conformational change observed in the heparin-binding pocket of the hFGF1 model in the absence of the heparin is directly linked to the thermal instability displayed by unbound monomeric hFGF1 experimentally. In addition to the intermolecular interactions between hFGF1 and heparin hexasaccharide, we have

https://doi.org/10.1021/acs.jpcb.1c07772
J. Phys. Chem. B 2021, 125, 12690−12697

identified several intramolecular interactions within the heparin-binding pocket that are unique to the heparin-bound models. Thermal denaturation experiments have revealed that the T_m value for hFGF1 increases by approximately 20 °C when bound to heparin. This suggests that the intramolecular interactions play a key role in stabilizing monomeric hFGF1. Further experimental and computational research is needed to elucidate the functional relevance of these specific intramolecular interactions.

■ ASSOCIATED CONTENT

Supporting Information

The Supporting Information is available free of charge at https://pubs.acs.org/doi/10.1021/acs.jpcb.1c07772.

Results of additional analyses; cartoon representation of dimeric hFGF1 with heparin; stability of heparin-bound hFGF1 RMSD/RMSF; salt-bridge analysis for heparin-bound models; intramolecular interactions in the heparin-binding pocket of heparin-bound Model 2; secondary structure analysis related to conformational change in *apo* model; behavior of heparin in both heparin-bound models; time series of hFGF1−heparin interactions (PDF)

■ AUTHOR INFORMATION

Corresponding Author

Mahmoud Moradi − *Department of Chemistry and Biochemistry, University of Arkansas, Fayetteville, Arkansas 72701, United States;* orcid.org/0000-0002-0601-402X; Email: moradi@uark.edu

Authors

Vivek Govind Kumar − *Department of Chemistry and Biochemistry, University of Arkansas, Fayetteville, Arkansas 72701, United States*

Shilpi Agrawal − *Department of Chemistry and Biochemistry, University of Arkansas, Fayetteville, Arkansas 72701, United States*

Thallapuranam Krishnaswamy Suresh Kumar − *Department of Chemistry and Biochemistry, University of Arkansas, Fayetteville, Arkansas 72701, United States*

Complete contact information is available at: https://pubs.acs.org/10.1021/acs.jpcb.1c07772

Author Contributions

M.M. and T.K.S.K. designed the research. V.G.K conducted the simulations and analyzed the simulation data. S.A. conducted the experiments and analyzed the experimental data. V.G.K, M.M., T.K.S.K., and S.A. wrote the manuscript.

Notes

The authors declare no competing financial interest.
All data will be shared upon request to corresponding author.

■ ACKNOWLEDGMENTS

This research is supported by National Science Foundation grant CHE 1945465 and OAC 1940188 and the Arkansas Biosciences Institute. Anton 2 computer time was provided by the Pittsburgh Supercomputing Center (PSC) through Grant R01GM116961 from the National Institutes of Health. The Anton 2 machine at PSC was generously made available by D. E. Shaw Research. This research is also part of the Blue Waters sustained-petascale computing project, which is supported by the National Science Foundation (awards OCI-0725070 and ACI-1238993) and the state of Illinois. This work also used the Extreme Science and Engineering Discovery Environment (allocation MCB150129), which is supported by National Science Foundation grant number ACI-1548562. This research is also supported by the Arkansas High Performance Computing Center, which is funded through multiple National Science Foundation grants and the Arkansas Economic Development Commission. This work is also supported by the Department of Energy (DE-FG02-01ER15161), the National Institutes of Health/National Cancer Institute (NIH/NCI) (1 RO1 CA 172631) and the NIH through the COBRE program (P30 GM103450).

■ REFERENCES

(1) Kim, J. Y.; Kim, C.; Lee, N. K. Real-Time Submillisecond Single-Molecule FRET Dynamics of Freely Diffusing Molecules with Liposome Tethering. *Nat. Commun.* **2015**, *6*, 6992.

(2) Srivastava, A.; Nagai, T.; Srivastava, A.; Miyashita, O.; Tama, F. Role of Computational Methods in Going beyond X-Ray Crystallography to Explore Protein Structure and Dynamics. *Int. J. Mol. Sci.* **2018**, *19*, 3401.

(3) Aduri, N. G.; Prabhala, B. K.; Ernst, H. A.; Jørgensen, F. S.; Olsen, L.; Mirza, O. Salt Bridge Swapping in the EXXERFXYY Motif of Proton-Coupled Oligopeptide Transporters. *J. Biol. Chem.* **2015**, *290*, 29931−29940.

(4) Doki, S.; Kato, H. E.; Solcan, N.; Iwaki, M.; Koyama, M.; Hattori, M.; Iwase, N.; Tsukazaki, T.; Sugita, Y.; Kandori, H.; et al. Structural Basis for Dynamic Mechanism of Proton-Coupled Symport by the Peptide Transporter POT. *Proc. Natl. Acad. Sci. U. S. A.* **2013**, *110*, 11343−11348.

(5) Immadisetty, K.; Hettige, J.; Moradi, M. What Can and Cannot Be Learned from Molecular Dynamics Simulations of Bacterial Proton-Coupled Oligopeptide Transporter GkPOT? *J. Phys. Chem. B* **2017**, *121*, 3644−3656.

(6) Bernett, M. J.; Somasundaram, T.; Blaber, M. An Atomic Resolution Structure for Human Fibroblast Growth Factor 1. *Proteins: Struct., Funct., Genet.* **2004**, *57*, 626−634.

(7) Eswarakumar, V. P.; Lax, I.; Schlessinger, J. Cellular Signaling by Fibroblast Growth Factor Receptors. *Cytokine Growth Factor Rev.* **2005**, *16*, 139−149.

(8) Beenken, A.; Mohammadi, M. The FGF Family: Biology, Pathophysiology and Therapy. *Nat. Rev. Drug Discovery* **2009**, *8*, 235−253.

(9) Kuro-o, M. Endocrine FGFs and Klothos: Emerging Concepts. *Trends Endocrinol. Metab.* **2008**, *19*, 239−245.

(10) Ornitz, D. M.; Herr, A. B.; Nilsson, M.; Westman, J.; Svahn, C. M.; Waksman, G. FGF Binding and FGF Receptor Activation by Synthetic Heparan-Derived Di- and Trisaccharides. *Science* **1995**, *268*, 432−436.

(11) Mohammadi, M.; Olsen, S. K.; Ibrahimi, O. A. Structural Basis for Fibroblast Growth Factor Receptor Activation. *Cytokine Growth Factor Rev.* **2005**, *16*, 107−137.

(12) Johnson, D. E.; Williams, L. T. Structural and Functional Diversity in the FGF Receptor Multigene Family. *Adv. Cancer Res.* **1992**, *60*, 1−41.

(13) Lin, X.; Buff, E. M.; Perrimon, N.; Michelson, A. M. Heparan Sulfate Proteoglycans Are Essential for FGF Receptor Signaling during Drosophila Embryonic Development. *Development* **1999**, *126*, 3715−3723.

(14) Yayon, A.; Klagsbrun, M.; Esko, J. D.; Leder, P.; Ornitz, D. M. Cell Surface, Heparin-like Molecules Are Required for Binding of Basic Fibroblast Growth Factor to Its High Affinity Receptor. *Cell* **1991**, *64*, 841−848.

(15) Rapraeger, A. C.; Krufka, A.; Olwin, B. B. Requirement of Heparan Sulfate for BFGF-Mediated Fibroblast Growth and Myoblast Differentiation. *Science* **1991**, *252*, 1705−1708.

(16) Taipale, J.; Keski-Oja, J. Growth Factors in the Extracellular Matrix. *FASEB J.* **1997**, *11*, 51−59.
(17) McKeehan, W. L.; Wang, F.; Kan, M. The Heparan Sulfate-Fibroblast Growth Factor Family: Diversity of Structure and Function. *Prog. Nucleic Acid Res. Mol. Biol.* **1997**, *59*, 135−176.
(18) Culajay, J. F.; Blaber, S. I.; Khurana, A.; Blaber, M. Thermodynamic Characterization of Mutants of Human Fibroblast Growth Factor 1 with an Increased Physiological Half-Life. *Biochemistry* **2000**, *39*, 7153−7158.
(19) Agostino, M.; Gandhi, N. S.; Mancera, R. L. Development and Application of Site Mapping Methods for the Design of Glycosaminoglycans. *Glycobiology* **2014**, *24*, 840−851.
(20) Imberty, A.; Lortat-Jacob, H.; Pérez, S. Structural View of Glycosaminoglycan-Protein Interactions. *Carbohydr. Res.* **2007**, *342*, 430−439.
(21) ten Dam, G. B.; Van De Westerlo, E. M. A.; Smetsers, T. F. C. M.; Willemse, M.; Van Muijen, G. N. P.; Merry, C. L. R.; Gallagher, J. T.; Kim, Y. S.; Van Kuppevelt, T. H. Detection of 2-*O*-Suifated Iduronate and N-Acetylglucosamine Units in Heparan Sulfate by an Antibody Selected against Acharan Sulfate (IdoA2S-GlcNAc)N. *J. Biol. Chem.* **2004**, *279*, 38346−38352.
(22) Babik, S.; Samsonov, S. A.; Pisabarro, M. T. Computational Drill down on FGF1-Heparin Interactions through Methodological Evaluation. *Glycoconjugate J.* **2017**, *34*, 427−440.
(23) Muñoz-García, J. C.; García-Jiménez, M. J.; Carrero, P.; Canales, A.; Jiménez-Barbero, J.; Martín-Lomas, M.; Imberty, A.; de Paz, J. L.; Angulo, J.; Lortat-Jacob, H.; et al. Importance of the Polarity of the Glycosaminoglycan Chain on the Interaction with FGF-1. *Glycobiology* **2014**, *24*, 1004−1009.
(24) Raman, R.; Venkataraman, G.; Ernst, S.; Sasisekharan, V.; Sasisekharan, R. Structural Specificity of Heparin Binding in the Fibroblast Growth Factor Family of Proteins. *Proc. Natl. Acad. Sci. U. S. A.* **2003**, *100*, 2357−2362.
(25) Habuchi, H.; Habuchi, O.; Kimata, K. Sulfation Pattern in Glycosaminoglycan: Does It Have a Code? *Glycoconjugate J.* **2004**, *21*, 47−52.
(26) Gama, C. I.; Tully, S. E.; Sotogaku, N.; Clark, P. M.; Rawat, M.; Vaidehi, N.; Goddard, W. A.; Nishi, A.; Hsieh-Wilson, L. C. Sulfation Patterns of Glycosaminoglycans Encode Molecular Recognition and Activity. *Nat. Chem. Biol.* **2006**, *2*, 467−473.
(27) Saxena, K.; Schieborr, U.; Anderka, O.; Duchardt-Ferner, E.; Elshorst, B.; Gande, S. L.; Janzon, J.; Kudlinzki, D.; Sreeramulu, S.; Dreyer, M. K.; et al. Influence of Heparin Mimetics on Assembly of the FGF·FGFR4 Signaling Complex. *J. Biol. Chem.* **2010**, *285*, 26628−26640.
(28) DiGabriele, A. D.; Lax, I.; Chen, D. I.; Svahn, C. M.; Jaye, M.; Schlessinger, J.; Hendrickson, W. A. Structure of a Heparin-Linked Biologically Active Dimer of Fibroblast Growth Factor. *Nature* **1998**, *393*, 812−817.
(29) Zhu, X. T.; Hsu, B. T.; Rees, D. C. Structural Studies of The Binding of The Antiulcer Drug Sucrose Octasulfate to Acidic Fibroblast Growth-Factor. *Structure* **1993**, *1*, 27−34.
(30) Canales, A.; Lozano, R.; López-Méndez, B.; Angulo, J.; Ojeda, R.; Nieto, P. M.; Martín-Lomas, M.; Giménez-Gallego, G.; Jiménez-Barbero, J. Solution NMR Structure of a Human FGF-1 Monomer, Activated by a Hexasaccharide Heparin-Analogue. *FEBS J.* **2006**, *273*, 4716−4727.
(31) Copeland, R. A.; Ji, H.; Halfpenny, A. J.; Williams, R. W.; Thompson, K. C.; Herber, W. K.; Thomas, K. A.; Bruner, M. W.; Ryan, J. A.; Marquis-Omer, D.; et al. The Structure of Human Acidic Fibroblast Growth Factor and Its Interaction with Heparin. *Arch. Biochem. Biophys.* **1991**, *289*, 53−61.
(32) Blaber, M.; Adamek, D. H.; Popovic, A.; Blaber, S. I. Biophysical and Structural Analysis of Human Acidic Fibroblast Growth Factor. *Technol. Protein Chem.* **1997**, *8*, 745−753.
(33) Carter, E. P.; Fearon, A. E.; Grose, R. P. Careless Talk Costs Lives: Fibroblast Growth Factor Receptor Signalling and the Consequences of Pathway Malfunction. *Trends Cell Biol.* **2015**, *25*, 221−233.
(34) Goetz, R.; Mohammadi, M. Exploring Mechanisms of FGF Signalling through the Lens of Structural Biology. *Nat. Rev. Mol. Cell Biol.* **2013**, *14*, 166−180.
(35) Phillips, J. C.; Braun, R.; Wang, W.; Gumbart, J.; Tajkhorshid, E.; Villa, E.; Chipot, C.; Skeel, R. D.; Kalé, L.; Schulten, K. Scalable Molecular Dynamics with NAMD. *J. Comput. Chem.* **2005**, *26*, 1781−1802.
(36) Best, R. B.; Zhu, X.; Shim, J.; Lopes, P. E. M.; Mittal, J.; Feig, M.; MacKerell, A. D. Optimization of the Additive CHARMM All-Atom Protein Force Field Targeting Improved Sampling of the Backbone φ, ψ and Side-Chain X1 and X2 Dihedral Angles. *J. Chem. Theory Comput.* **2012**, *8*, 3257−3273.
(37) Jo, S.; Kim, T.; Im, W. Automated Builder and Database of Protein/Membrane Complexes for Molecular Dynamics Simulations. *PLoS One* **2007**, *2*, No. e880.
(38) Lee, J.; Cheng, X.; Swails, J. M.; Yeom, M. S.; Eastman, P. K.; Lemkul, J. A.; Wei, S.; Buckner, J.; Jeong, J. C.; Qi, Y.; et al. CHARMM-GUI Input Generator for NAMD, GROMACS, AMBER, OpenMM, and CHARMM/OpenMM Simulations Using the CHARMM36 Additive Force Field. *J. Chem. Theory Comput.* **2016**, *12*, 405−413.
(39) Reid, J. K., Ed. *Large Sparse Sets of Linear Equations*; Academic Press: London, 1971.
(40) Martyna, G. J.; Tobias, D. J.; Klein, M. L. Constant Pressure Molecular Dynamics Algorithms. *J. Chem. Phys.* **1994**, *101*, 4177−4189.
(41) Darden, T.; York, D.; Pedersen, L. Particle Mesh Ewald: An N·log(N) Method for Ewald Sums in Large Systems. *J. Chem. Phys.* **1993**, *98*, 10089−10092.
(42) Humphrey, W.; Dalke, A.; Schulten, K. VMD: Visual Molecular Dynamics. *J. Mol. Graphics* **1996**, *14*, 33−38.

https://doi.org/10.1021/acs.jpcb.1c07772
J. Phys. Chem. B 2021, 125, 12690−12697